ACS APPLIED MATERIALS & INTERFACES

www.acsami.org

Research Article

Constructing an Al^{3+}/Zn^{2+}-Based Solid Electrolyte Interphase to Enable Extraordinarily Stable Al^{3+}-Based Electrochromic Devices

Shichen Weng, Zhenhu Cao, Kunrun Song, Wentao Chen, Ran Jiang, Alexandr Alexandrovich Rogachev, Maxim Anatolievich Yarmolenko, Jumei Zhou,* and Hongliang Zhang*

Cite This: *ACS Appl. Mater. Interfaces* 2024, 16, 18164−18172

Read Online

ACCESS | Metrics & More | Article Recommendations | Supporting Information

ABSTRACT: The interface between the electrochromic (EC) electrode and ionic conductor is crucial for high-performance and extraordinarily stable EC devices (ECDs). Herein, the effect of the ALD−AZO interfacial layer on the performance of the WO_3 thin film was examined, revealing that an introduction of the ALD−AZO interfacial layer to the Al^{3+}-based complementary ECDs can lead to improved EC performance and stability, such as an extraordinary cyclability of more than 20,000 cycles, an outstanding coloration efficiency of 109.69 cm^2 C^{-1}, and a maximum transmittance modulation of 63.44%@633 nm. The probable explanation is that the introduced ALD−AZO interfacial layer can effectively regulate the band gap of WO_3, promote the electron transport process, and induce the formation of a robust solid electrolyte interphase to protect the electrode during cycling. These findings offer valuable insights for enhancing the EC performance of the EC thin films and new space for the construction of advanced multivalent Al^{3+}-based ECDs.

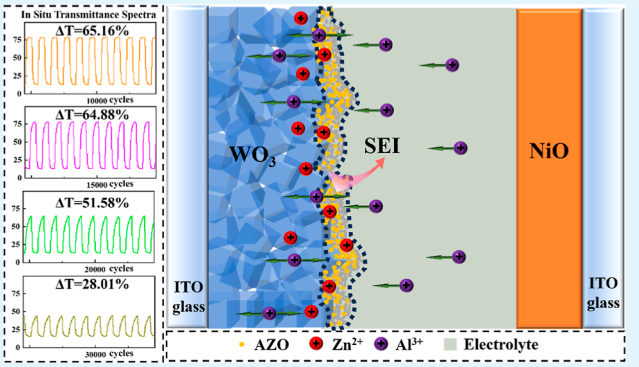

KEYWORDS: *electrochromism, atomic layer deposition, solid electrolyte interphase, tungsten oxide, multivalent ions*

1. INTRODUCTION

Electrochromic materials (ECMs) are defined as those with reversible changes in their colors and optical properties (absorbance/transmittance/reflectance) via a redox reaction by a small applied voltage.[1] ECMs have undergone thorough examination for numerous potential applications, including rear-view mirrors, electrochromic (EC) smart windows in buildings, and automotive sunroofs, due to their low power consumption and significant transmittance contrast. Tungsten oxide (WO_3) is considered one of the most promising ECMs as the EC layer of EC devices (ECDs) owing to its simple preparation process and high coloration efficiency.[2,3] Typical WO_3−NiO ECDs consist of five layers: a WO_3 thin film (EC layer), an ion-conducting layer, a NiO thin film (ion-storage layer), and transparent electrodes on both sides.[4−7] Conventionally, the monovalent Li^+ is used as the mainstream conducting ions of the electrolytes for the ECDs because of its small ionic radii, which is beneficial to the insertion and extraction processes between the layers. However, Li^+ still has disadvantages that limit its practical use, including the environmental issues related to lithium usage and the limited lithium salt resources.[8−10]

In the field of ECDs, the use of multivalent conducting cations such as Al^{3+}, Zn^{2+}, or Mg^{2+} is highly attractive. These cations provide multiple charges for the electrolytes during redox reactions, enabling a high capacity and fast switching speed. Among them, Al^{3+} has been studied extensively due to its small ionic radius (0.053 nm), high charge, and natural abundance.[11,12] Zhang et al. have shown that using Al^{3+} as transport ions can result in high optical modulation, fast response, and long-term stability for the WO_3 EC electrodes.[13] Unfortunately, the disadvantages of Al, such as its tendency to passivate easily and its high redox potential, have posed challenges for its further development. For instance, Al^{3+} has been regarded as a notably poor migrant in solids due to its substantial electrostatic interaction with surrounding anionic structures and the low polarizability of the ion caused by a small Al^{3+} ionic radius.[14,15] On the other hand, Zn metal possesses numerous benefits including a low redox potential (−0.76 vs SHE), environmental compatibility, and safety. Zn metal can be used as the ion-storage layer for the EC layer of ECDs.[16] The higher Gibbs free energy of EC materials compared with that of the Zn foil leads to self-coloration of the ECDs during the discharge process. It is reported that the Zn^{2+}-based ECD using the WO_3 and Zn metal electrodes

Received: January 6, 2024
Revised: March 18, 2024
Accepted: March 22, 2024
Published: April 1, 2024

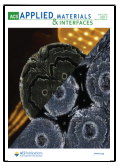

exhibits large optical transmittance (76%) and good continuous cycling stability. However, the development of Zn^{2+}-based ECDs is significantly limited by several factors, such as high interface activation energy and low electrochemical activities. Recent research has shown promising results for the hydrogel-electrolyte quasi-solid-state WO_3/Zn ECD using a Zn^{2+}/Al^{3+} hybrid electrolyte, exhibiting a remarkable ion conductivity of 20 mS cm^{-1}.[17] Wu et al. developed a high-performance ECD using WO_3 and Zn as the electrodes in a hybrid Zn^{2+}/Al^{3+} electrolyte. This novel ECD possesses impressive characteristics, including a rapid self-coloring response time of 10.8 s, a high optical modulation of 90.5%, and an excellent cyclic stability of up to 5000 cycles with 93.13% retention.[18] To further improve the EC performance of the electrode materials for ECDs using Al^{3+} as the transport ions, a robust hybrid Al^{3+}/Zn^{2+}-based interface is being explored as it is expected to provide additional enhancement possibilities.

Herein, we have made significant advancements in the field of electrochromism by depositing an ultrathin layer of AZO using atomic layer deposition (ALD) on the WO_3 thin film. This is the first time that such a combination has been explored in electrochromism. Through electrochemical tests, UPS, and optical tests, we demonstrate the significant enhancement of cycling stability and electrochemical performance for WO_3 facilitated by the Al^{3+}/Zn^{2+}-based solid electrolyte interphase (SEI), as shown in Scheme 1. To determine the components of the robust Al^{3+}/Zn^{2+}-based SEI, we employed X-ray photoelectron spectroscopy (XPS), transmission electron microscopy (TEM), and scanning electron microscopy (SEM) techniques. Moreover, the assembled complementary WO_3/AZO-NiO ECD based on the Al^{3+}-electrolyte exhibits an extraordinarily stable cyclic performance, sustaining over 20,000 cycles, indicating its long-term stability. Additionally, the ECD demonstrates an impressive coloration efficiency of 109.69 cm^2 C^{-1} and a maximum transmittance modulation of 63.44%@633 nm.

Scheme 1. Scheme of the AZO/WO_3−NiO ECD

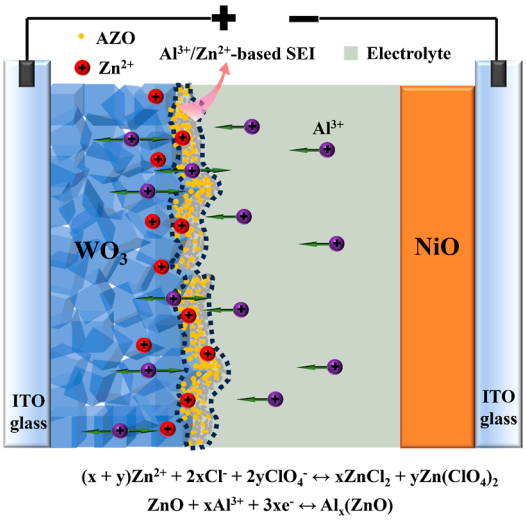

2. EXPERIMENTAL SECTION

2.1. Preparation of Thin Films and Assembly of ECDs. The details of the deposition equipment are listed in Table S1. The ITO glass substrates were used for the deposition of the WO_3 and NiO thin films, and the deposition process and characteristics of the thin films are described in S1. AZO was directly deposited on WO_3 thin films at a substrate temperature of 150 °C using thermal ALD. Trimethylaluminum ($Al(CH_3)_3$, TMA), diethylzinc ($Zn(C_2H_5)_2$, DEZ), and H_2O served as the precursor materials. These precursors were sequentially introduced into the reaction chamber by pure N_2 (7 sccm).[19,20] Each ALD included four steps: (i) pulse of DEZ/TMA (0.02 s), (ii) N_2 purge (20 s), (iii) pulse of H_2O (0.015 s), and (iv) N_2 purge (20 s). One TMA cycle was inserted after 19 DEZ cycles.

The assembly of the ECD was completed through the vacuum filling process. 0.1 M PC-$Al(ClO_4)_3$ was injected between the AZO/WO_3 working electrode and NiO counter electrode. The structure of the ECD can be described as ITO/WO_3/AZO/PC-$Al(ClO_4)_3$/NiO/ITO. The experimental results show that $Al(ClO_4)_3$ used in our experiment can be transformed into $Al(ClO_4)_3{\cdot}9H_2O$ after absorbing water molecules (such as exposure to air). Fortunately, $Al(ClO_4)_3$ was dissolved in the PC solvent, thus isolating the air. This greatly reduces the risk of its transformation into $Al(ClO_4)_3{\cdot}9H_2O$.

2.2. Characterization. The instrument types and test conditions are listed in Table S1. X-ray diffraction (XRD), TEM, and SEM were used to analyze the morphology and microstructure of the thin films. The in situ transmittance spectra were acquired using both visible spectroscopy and an electrochemical workstation. X-ray photoelectron spectroscopy was used to detect the surface chemical state. The details regarding XPS measurements and analysis are shown in S1. Cyclic voltammetry (CV), galvanostatic charge−discharge, and electrochemical impedance spectroscopy (EIS) were conducted using the electrochemical workstations. Notably, the electrochemical tests of thin films were performed in a three-electrode cell with 0.1 M PC-$Al(ClO_4)_3$ as the electrolyte (Supporting Information S1).

3. RESULTS AND DISCUSSION

3.1. EC Performance of the Thin Films. The in situ visible transmittance spectra at a wavelength of 633 nm for the ALD−AZO/WO_3 and WO_3 thin films are obtained by the applied voltage (−1.0 and 1.0 V). It can be seen that the maximum transmittance modulation (ΔT) of the AZO/WO_3 thin film shows a small decay (only about 2%) after continuous cycling for 1000 cycles (60,000 s), showing better EC stability compared with that of the WO_3 thin film. The colored/bleached response times (the time required to achieve a 90% change in transmittance between the colored and bleached states) are estimated to be about 7.1 s/9.8 s and 10.2 s/11.7 s for the AZO/WO_3 and WO_3 thin films, respectively (Figure 1b).[21] Remarkably, the colored/bleached response time of the AZO/WO_3 thin film after 1000 cycles is measured to be 5.9 s/7.8 s. Figures 1c and S1a show, respectively, the ex situ optical transmittance spectra of the AZO/WO_3 and WO_3 thin films, revealing a high optical modulation of 92.31 and 92.36% at λ_{633nm}. Moreover, the optical band gap of the thin films is determined by fitting the absorption spectra, as shown in Figure 1d. The optical band gap can be calculated according to the following equation

$$\alpha h\nu = A(h\nu - E_g)^2 \quad (1)$$

where α is the absorption coefficient, h is the Planck constant, ν is the light frequency, A is a proportionality constant, and E_g is the optical band gap.[22] Based on the equation, the band gap of the AZO/WO_3 and WO_3 thin films is calculated to be 3.01 and 3.37 eV, respectively. To further reveal the reason the AZO/WO_3 thin films have a faster response time and narrower optical band gap, UV photoelectron spectroscopy (UPS) is applied to quantitative analysis for the Fermi energy (E_f), cutoff energy (E_{cutoff}), and work functions (Φ), as shown in Figure S1b. The calculated Φ values of the AZO/WO_3 and

https://doi.org/10.1021/acsami.4c00303
ACS Appl. Mater. Interfaces 2024, 16, 18164−18172

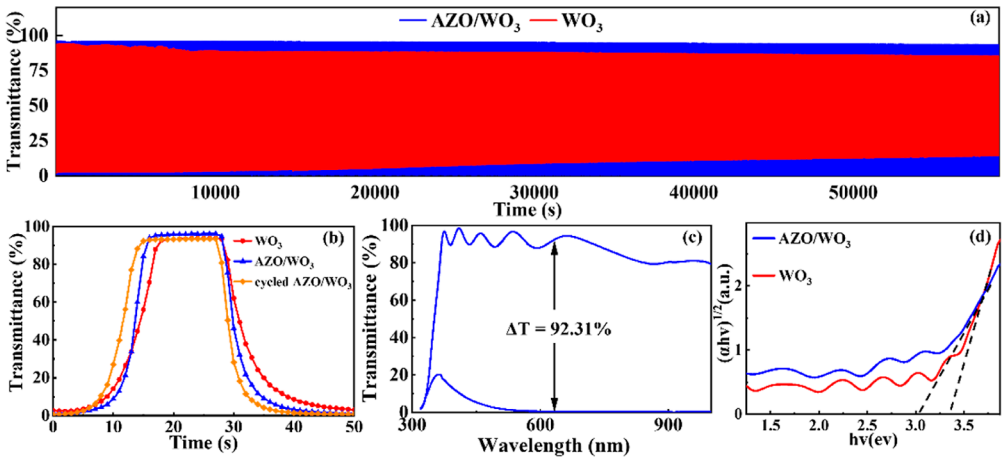

Figure 1. (a) In situ visible transmittance spectra at a wavelength of 633 nm for thin films. (b) Response times of thin films. (c) Ex situ optical transmittance spectra of the ALD−AZO/WO_3 thin film. (d) $(\alpha h\nu)^{1/2}$ vs photon energy ($h\nu$) plots for thin films.

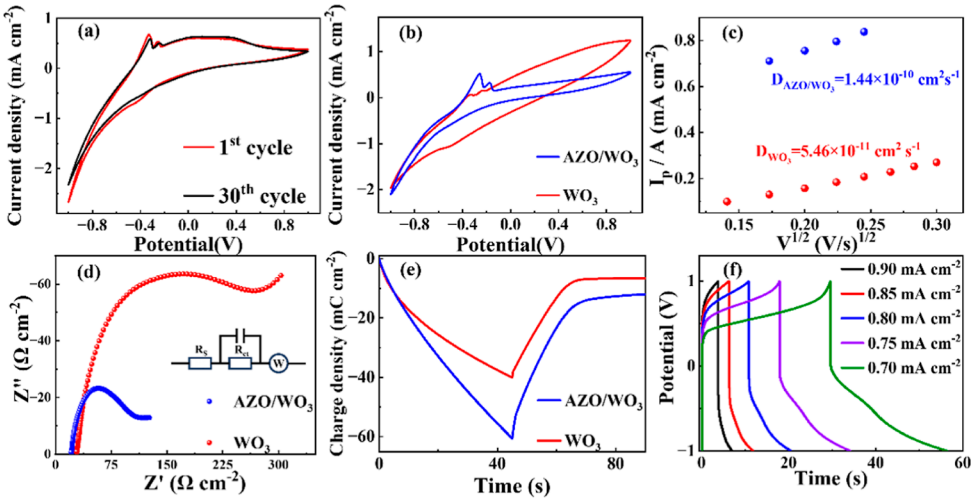

Figure 2. (a) CV curves at the 1st and 30th cycles of the ALD−AZO/WO_3 thin film. (b) CV curves of the ALD−AZO/WO_3 and WO_3 thin films. (c) Dependence of the peak current densities (I_p) vs the square root of the scan rate ($v^{1/2}$) for thin films. (d) Nyquist plot for thin films. (e) Charge densities of thin films. (f) Charge/discharge curves for the ALD−AZO/WO_3 thin film at different current densities.

WO_3 thin films are 7.12 and 7.95 eV, respectively. The lower Φ of the AZO/WO_3 thin films is expected to promote the electron transport process, which can contribute to better electrochemical performance.[23,24]

3.2. Electrochemical Performance of the Thin Films. The CV test is a commonly used method to evaluate the electrochemical activity and the ion intercalation processes in thin films. In our case, the CV curves of the ALD−AZO/WO_3 thin films were examined in comparison to those of the bare WO_3 thin films. Figure 2a shows the 1st and 30th CV curves of the AZO/WO_3 thin film. At the first cycle, there is a broad reduction peak between −0.35 and −0.45 V, which is attributed to the sacrificial decompositions of electrolyte components (PC) and the formation of the SEI.[25,26] It can be seen that the reduction peak disappears in the 30th cycle, indicating the irreversibility of SEI formation. The presence of the ALD−AZO coating can accelerate densification of the SEI and the constraints it imposes on the reaction product formation.[27,28] Figure 2b compares the CV curves of the AZO/WO_3 and WO_3 thin films. It can be clearly seen that there are two oxidation peaks located between 0.1 and 0.3 V, which can be attributed to the multistep deintercalation of the multivalent cation (Al^{3+}).[29] The AZO/WO_3 thin film exhibits higher current densities compared with those of the WO_3 thin film, revealing that it is more electrochemically active toward Al^{3+} ions. This suggests that the addition of the ALD−AZO interfacial layer enhances the electrochemical reactivity of the WO_3 thin film. The aforementioned UPS results indicate that the introduction of AZO promotes charge transfer at the interface between the WO_3 electrode and the electrolyte. The findings from UPS are consistent with the fact that oxidation reactions contribute to the two more obvious peaks of the AZO/WO_3 thin films in the CV curves than that of the WO_3 thin film. These findings do not rule out the influence of the SEI of the AZO/WO_3 thin film, which effectively prevents several negative side reactions during cycling. This results in a reduced contribution to the current from side reactions. Therefore, the CV curve area of the AZO/WO_3 thin film is smaller than that of the WO_3 thin film. To determine the ion diffusion coefficient, the CV current densities of the different scan rates for the thin films at different scan rates from 10 to 100 mV s^{-1} were analyzed (Figure S2a,b). The ion diffusion coefficient can be calculated according to the following Rand−Sevcik equation

https://doi.org/10.1021/acsami.4c00303
ACS Appl. Mater. Interfaces 2024, 16, 18164−18172

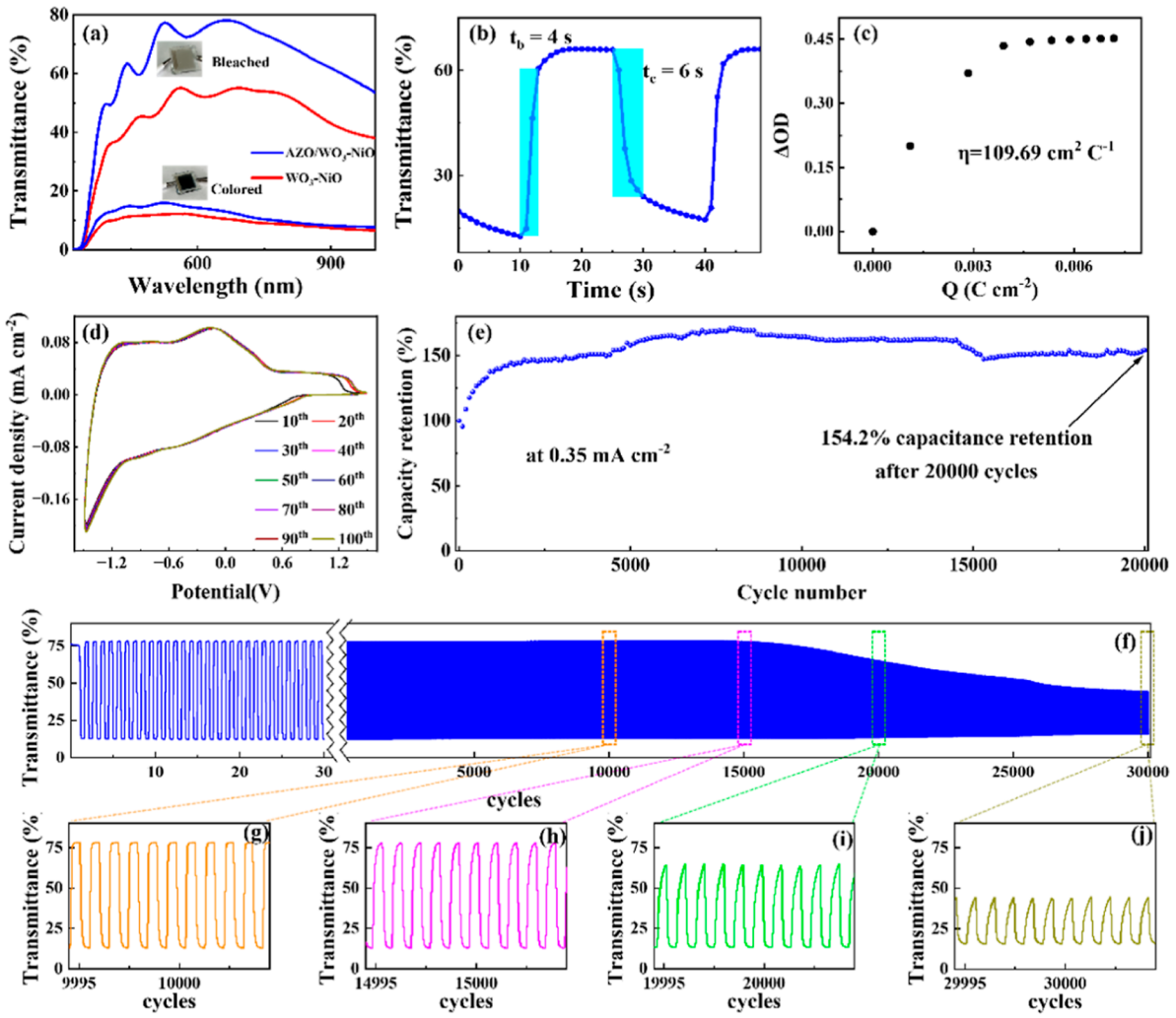

Figure 3. (a) Ex situ transmittance spectra, (b) response times, (c) plots of in situ optical density variation as a function of charge density, (d) 100 CV curves, and (e) cyclic performance for the ECD. (f) In situ visible transmittance spectra at a wavelength of 633 nm for the ECD. The ΔT of the ECD for the (g) 10,000th, (h) 15,000th, (i) 20,000th, and (j) 30,000th cycles.

$$I_p = 2.72 \times 10^5 \times n^{3/2} \times A \times D^{1/2} \times C_0 \times v^{1/2} \quad (2)$$

where I_p is the peak current and n, A, D, C_0, and v are the number of electrons participating in the reactions, the contact area between the electrolyte and electrode, the diffusion coefficient of ions, the ion concentration in the electrolyte, and the scan rate, respectively.[30] As shown in Figure 2c, the ion diffusion coefficient of the WO_3 thin films with the ALD−AZO interfacial layer (1.44×10^{-10} cm^2 s^{-1}) is significantly larger than that of the WO_3 thin films (5.46×10^{-11} cm^2 s^{-1}). Generally, the rate performance of EC thin films primarily hinges on the diffusion coefficient and distance. The larger D value of the AZO/WO_3 thin film is consistent with times observed in Figure 1b. Moreover, the charge transfer resistance (R_{ct}) of the AZO/WO_3 and WO_3 thin films is measured to be 56.7 and 126.3 Ω cm^{-2}, respectively, as shown in the Nyquist plot (Figure 2d). The smaller R_{ct} of the AZO/WO_3 thin film indicates less obstruction to reactions at the electrode/electrolyte interface compared with the bare WO_3 thin film. The modification of the ALD−AZO interfacial layer effectively improves the reaction kinetics of the WO_3 thin films, which is confirmed by the results of the CV and EIS. The charge density of the AZO/WO_3 and WO_3 thin films is calculated to be 60.64 and 40.06 mC cm^{-2} by the chronocoulometry method, respectively (Figure 2e). The higher charge density observed in the AZO/WO_3 thin film can be attributed to the presence of the ALD−AZO interfacial layer, which contributes to capacitance during cycling. It is reported that ions can be stored reversibly in the grain boundary regions, which acts as an intermediary state between intercalation and storage in supercapacitors. This type of interfacial storage facilitates a rapid transfer and storage of ions.[31] Similarly, the AZO/WO_3 thin film exhibits comparable interfacial Al^{3+} storage. Besides, as illustrated in Figure 2f, the AZO/WO_3 thin film demonstrates cyclic charge/discharge curves with notable symmetry from 0.70 to 0.90 mA cm^{-2}, indicating a good reversibility of the AZO/WO_3 thin film.

3.3. EC and Electrochemical Performance of the Complementary ECDs. Figure 3a shows the ex situ transmittance spectra of the fabricated ECDs tested before long-term cycling. The details of NiO, which is the counter electrode for the WO_3 thin film, are shown in Supporting Information S4 and S5. The ΔT of the ECD using the ALD−AZO/WO_3 and bare WO_3 thin films as the working electrodes is measured to be 63.44 and 41.43%, respectively. The larger ΔT of the ECDs based on the AZO/WO_3 thin films can be

https://doi.org/10.1021/acsami.4c00303
ACS Appl. Mater. Interfaces 2024, 16, 18164−18172

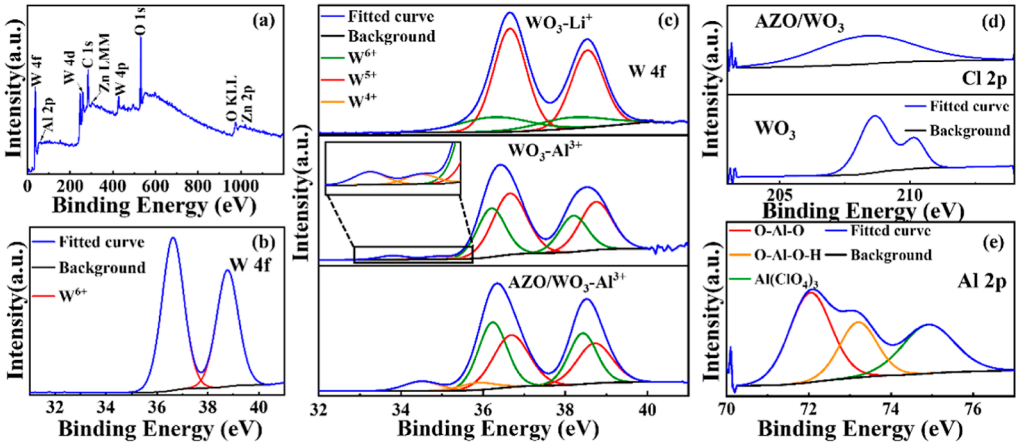

Figure 4. (a) XPS full-range spectra of the uncycled ALD−AZO/WO_3 thin film. (b) W 4f spectra of the uncycled WO_3 thin film. (c) W 4f spectra for the cycled WO_3 and AZO/WO_3 thin films using 0.1 M PC-$LiClO_4$ or 0.1 M PC-$Al(ClO_4)_3$. (d) Cl 2p spectra of the cycled ALD−AZO/WO_3 and WO_3 thin films. (e) Al 2p spectra for the cycled ALD−AZO/WO_3 thin film.

attributed to the higher electrochemical activity of the AZO/WO_3 thin film toward Al^{3+} compared with that of the WO_3 thin film. The colored/bleached response time of the ECD using the AZO/WO_3 thin film is estimated to be 6 s/4 s. The ECD is not ideal in the second cycle of the colored process. For higher voltage (>4.0 V)-driven lithium-ion batteries, SEI formation usually tends to be complete after 1 cycle.[26] In contrast, in ECDs driven by low voltage (<3.0 V), the activation process usually seems to be complete after a few (<10) cycles, and SEI formation occurs accordingly. This can be confirmed from the electrochemical (Figure 3e) and EC (Figure 3f) long-term stable performance of the ECDs. Therefore, the observed increase in the second cycle of the colored process can be attributed to the unfinished activation process and the SEI that is not yet fully formed. The coloration efficiency (η) of the ECDs using the AZO/WO_3 thin film is calculated to be 109.69 $cm^2\ C^{-1}$ (Figure 3b,c), better than the previous report.[6,13] Figure 3d illustrates a minimal alteration in the shape and alignment of the CV curves for the ECD using the AZO/WO_3 thin film at a scan rate of 50 mV s^{-1} over 100 cycles, indicating the good electrochemical stability of the ECD. Furthermore, the ECD using the AZO/WO_3 thin film shows extraordinarily stable cyclic performance with 154.2% capacitance retention after 20,000 consecutive cycles at a current density of 0.35 mA cm^{-2} (Figure 3e). The capacitance retention exceeding 100% can be attributed to the following reasons. (i) The formation of the loose structure for the cycled thin films facilitates direct contact between the electrolyte and active materials through penetration. (ii) The heightened charge density exchange observed in the NiO thin film over successive cycles results in an increased participation of Ni atoms in the EC reaction and the increase of the adsorption of anions (Al^{3+}) and cations (ClO_4^-).[32,33] The ΔT of the ECD drops from 65.46% for the first cycle to 51.58% for the 20,000th cycle, as shown in the in situ visible transmittance spectra of the ECD (Figure 3f,i), indicating an acceptable degradation. The longevity of the film after 20,000 cycles can be seen in Figure 3i, and the ΔT of the ECD drops from 51.58% for the 20,000th cycle to 28.01% for the 30,000th cycle. The observed degradation in optical modulation after the 20,000th cycle can be likely linked to the irreversible insertion and extraction process within the WO_3 EC layer, along with the instability of the interface. The outstanding long-term stability of the ECD using the AZO/WO_3 thin film can be attributed to two factors. First, the strong electrostatic force between aluminum ions and the electrode (including WO_3 and AZO) decreases the ion diffusion distance and relieves the structural collapse of the WO_3 framework.[6,29] Second, the ALD−AZO interfacial layer facilitates the formation of a stable and effective SEI between the electrode and electrolyte, leading to enhanced long-term stability. Besides, a comparison of stability between this work and other reported work is shown in Table S2. The ECDs fabricated in this study exhibit superior cyclic stability.

3.4. XPS of the Thin Films. Ex situ XPS analysis was conducted to investigate the interfacial layer formed on the ALD−AZO/WO_3 and bare WO_3 thin films. The XPS full-range spectra of the uncycled AZO/WO_3 thin film show distinct peaks corresponding to Zn and Al elements (Figure 4a). The W 4f XPS results indicate the dominance of W^{6+} in the uncycled WO_3 film,[34] with no observable peaks related to W^{5+} and W^{4+} (Figure 4b). The prepared WO_3 thin film is suitable for direct utilization as the EC layer, and W^{6+} can be reduced by the electrons generated in the colored process and Al^{3+}. Figure 4c compares the W 4f spectra of the cycled AZO/WO_3 and bare WO_3 thin films using 0.1 M PC-$LiClO_4$ or 0.1 M PC-$Al(ClO_4)_3$. The XPS results of the cycled thin films using 0.1 M PC-$Al(ClO_4)_3$ show the presence of W^{4+} peaks, whereas these peaks are not observed in the XPS results of the cycled thin film using 0.1 M PC-$LiClO_4$. This indicates that the WO_3 thin film demonstrates higher electrochemical activity toward a multivalent cation (Al^{3+}) compared with Li ions. Moreover, the area proportion of the W^{4+} peaks in the thin films cycled in 0.1 M PC-$Al(ClO_4)_3$ is calculated to be 3.18% for the bare WO_3 thin film and 8.20% for the AZO/WO_3 thin film. This further confirms the enhanced EC and electrochemical performance of the AZO/WO_3 thin film compared to that of the bare WO_3 thin film, consistent with the results presented in Figures 1 and 2. As shown in Figure 4d, a shifted broad peak is evident within the Cl 2p spectra of the cycled AZO/WO_3 thin film instead of two peaks in the Cl 2p spectra of the cycled WO_3 thin film. This indicates the participation of the ALD−AZO interfacial layer in the electrochemical reaction, which can lead to the presence of $ZnCl_2$ or $Zn(ClO_4)_2$.

https://doi.org/10.1021/acsami.4c00303
ACS Appl. Mater. Interfaces 2024, 16, 18164−18172

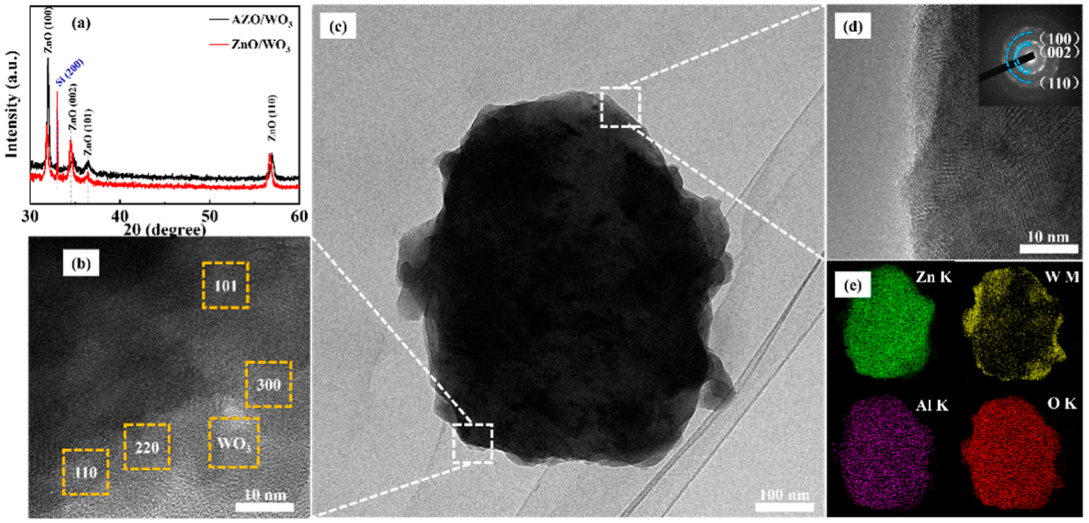

Figure 5. (a) XRD results for the ALD−AZO/WO_3 and ALD−ZnO/WO_3 thin films. (b−d) TEM images for the AZO/WO_3 thin film. (e) EDX mapping images for the ALD−AZO/WO_3 thin film.

The mechanisms of the intercalation of Al^{3+} ions passing through the ALD−AZO layer (Scheme 1) can be summarized as follows. (i) Al^{3+} ions pass partly through the ALD−AZO layer by pore diffusion.[26] (ii) Extra Al^{3+} ions overflow into the WO_3 thin film by passing through the ALD−AZO until reaching the thermodynamically stable state, as stated by Jung et al.[35] This reversible process is characterized by the following steps

$$(x + y)Zn^{2+} + 2xCl^{-} + 2yClO_4^{-} \leftrightarrow xZnCl_2 + yZn(ClO_4)_2 \quad (3)$$

$$ZnO + xAl^{3+} + 3xe^{-} \leftrightarrow Al_x(ZnO) \quad (4)$$

The Al 2p XPS spectra of the cycled AZO/WO_3 thin film display three peaks characteristic of O−Al−O, O−Al−O−H, and $Al(ClO_4)_3$ (Figure 4e). The C 1s spectra of the AZO/WO_3 thin film are similar to those of the WO_3 thin film, indicating that the SEI components related to the C element in the cycled AZO/WO_3 thin film are roughly the same as those in the cycled WO_3 thin film, including the electrolyte and its decomposition products. This is further demonstrated by the Raman results. As shown in Figure S5, the peak at 1093 cm^{-1} is evident in both spectra of the cycled AZO/WO_3 and WO_3 thin films. This peak is associated with the symmetric stretching vibration of the anion from $M_x(CO_3)_y$. $M_x(CO_3)_y$ constitutes an SEI product, resulting from the breakdown of organic carbonates within the electrolyte. The signals between 900 and 1150 cm^{-1} of the cycled thin films becoming sharper than those of the uncycled thin films can be attributed to the nondecomposed electrolyte and the stretching vibrations of R−O− and C−C− within the semicarbonates. The Raman results indicate that the effective components of the SEI are formed in both AZO/WO_3 and WO_3 thin films after electrochemical cycling in the $Al(ClO_4)_3$-PC electrolyte. Notably, the proportion of the O−C═O peak area in AZO/WO_3 is larger than that of bare WO_3 (Figures S6a and S6b). This can be ascribed to the faster SEI formation induced by the ALD−AZO interfacial layer, thereby diminishing the electrolyte breakdown while augmenting the organic component within the interface.[36,37] Hence, the Al^{3+}/Zn^{2+}-based SEI layer of the cycled AZO/WO_3 thin film is expected to consist of ALD−AZO and decomposition products of the electrolyte. Except for the AZO part, the XPS and Raman results indicate that the SEI components related to the C element in the cycled AZO/WO_3 thin film are roughly the same as those in the cycled WO_3 thin film. In fact, the films and ECDs based on the AZO/WO_3 electrodes show more excellent electrochemical (Figure 3e) and EC (Figure 3f) long-term stable performance than that of the bare WO_3 electrodes. A possible explanation for these results can be the lack of a robust AZO-based SEI of the WO_3 electrode and the $Al(ClO_4)_3$-PC electrolyte.

3.5. TEM of the Thin Films. Figure 5a shows the XRD patterns of the ALD−AZO/WO_3 thin films. The as-deposited WO_3 thin films possess an amorphous nature (Figure S4a). The pattern of the AZO/WO_3 thin film shows four peaks corresponding to the (100), (002), (101), and (110) planes of AZO. The peaks, except the (100) peak, have reduced intensities and are slightly shifted toward larger diffraction angles. The presence of amorphous alumina and the substitution of Zn^{2+} by Al^{3+} ions can account for these changes, which lead to increased lattice disorder and a decrease in the crystalline lattice constant. The findings are consistent with previous reports.[38,39] The inverse fast Fourier transform (FFT) technique, utilizing Digital Micrograph, is utilized to isolate and filter the square region corresponding to the AZO/WO_3 thin film. The high-resolution TEM (HRTEM) image reveals lattice fringes of 0.169, 0.078, 0.092, and 0.240 nm. The corresponding FFT images (Figure S7) display bright spots that can be associated with the (110), (220), (300), and (101) planes of AZO, respectively. In contrast, Figure S7f depicts the HRTEM image where no lattice fringes are found, accompanied by an FFT image showing only a halo background. These findings indicate the amorphous nature of WO_3 in this region. Moreover, the inset depicting the selected area electron diffraction image of the AZO/WO_3 film illustrates rings assigned to the (100), (002), and (110) planes of AZO (Figure 5d). Furthermore, the mapping images obtained from energy-dispersive X-ray spectroscopy (EDX) analysis (Figures 5e and S8) confirm the presence and homogeneous distribution of Zn, W, Al, and O elements across the AZO/WO_3 thin film. Taken together, these results demonstrate that the structure of the

https://doi.org/10.1021/acsami.4c00303
ACS Appl. Mater. Interfaces 2024, 16, 18164−18172

AZO/WO_3 film consists of an amorphous WO_3 thin film and an ultrathin polycrystalline ALD−AZO coating.

3.6. SEM of the Films. Figure 6a shows the SEM image of the surface for the uncycled AZO/WO_3 thin film. It can be observed that the thin film is composed of densely arranged nanoparticles, with no significant difference compared to the WO_3 thin film (Figure S9a). This indicates that the introduction of the ALD−AZO interfacial layer at an approximate thickness can greatly enhance the electrochemical and EC performance of the WO_3 working electrodes without hindering the transport of ions. In Figure 6b, the SEM image of the AZO/WO_3 thin film after 1000 cycles with the applied voltage (−1.0 and 1.0 V) displays a porous and loose surface morphology. This can be attributed to the expansion and contraction of the AZO interfacial layer and surface WO_3 during cycling. The formation of this loose structure facilitates direct contact between the electrolyte and active materials through penetration, leading to adverse reactions such as further electrolyte breakdown and WO_3 leaching.[36,40,41] Remarkably, unlike that of the AZO/WO_3 thin film, the SEM image of the WO_3 thin film after cycling shows obvious cracks on the surface (Figure S9b). This corresponds to a more significant decrease in EC performance compared with that of the AZO/WO_3 thin film (Figure 1). The pristine WO_3 unveiled by the cracks generated throughout the reaction instigated the genesis of a fresh interface. Moreover, ALD−AZO mitigates the incidence of minor cracks, the primary catalysts for widespread clefting.[42] As shown in Figure S10a,b, the values of the root-mean-square roughness for the uncycled AZO/WO_3 and WO_3 thin films are 2.51 and 3.21 nm, respectively. It seems possible that the small roughness value can be ascribed to the flat surface of the WO_3 thin films composed of densely arranged nanoparticles and the completely conformal coating of ALD−AZO on WO_3. A possible explanation for the smaller roughness of the uncycled AZO/WO_3 thin film can be the reduction of small cracks and pinholes of the WO_3 thin film by means of the coverage of ALD−AZO. In Figure S10c,d, it is observed that the roughness of the AZO/WO_3 and WO_3 thin films measures 2.63 and 3.69 nm after 50 electrochemical cycles, respectively. The observed increase in roughness of the cycled thin film cannot rule out structural change originated from ion intercalation/deintercalation and SEI formation.

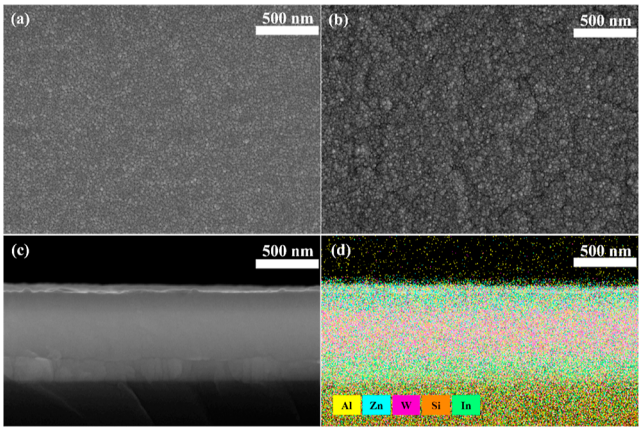

Figure 6. Surface SEM micrograph of the (a) uncycled and (b) cycled ALD−AZO/WO_3 thin films. (c) Cross-section SEM micrograph of the AZO/WO_3 thin film with a 50 nm thick ALD−AZO interfacial layer. (d) EDS mapping result of the AZO/WO_3 thin film with a 50 nm thick ALD−AZO interfacial layer.

By increasing the number of ALD−AZO cycles, the WO_3 surface is completely covered with a continuous layer (Figure S9c). The WO_3 thin film with a 50 nm-thick ALD−AZO interfacial layer is used for obtaining a clear ALD−AZO/WO_3 interface of the cross-section SEM micrograph (Figure 6c). Lots of obvious nanoparticles can be observed, in agreement with those of the previously reported ALD−AZO. Additionally, the cross-section energy-dispersive spectrometry (EDS) mapping result of elements in the AZO/WO_3 thin film with a 50 nm-thick ALD−AZO interfacial layer is shown in Figure 6d, indicating the detection of Zn and Al elements in both the surface and entire thickness range of the thin film. The ALD−AZO coating on the surface, along with the Al/Zn structure embedded within the thin film, can enhance the electrical conductivity of the WO_3 thin film and improve reaction kinetics and cycling stability. Furthermore, in consideration of the thin film tested in the Al-based electrolyte, the inclusion of Al within the WO_3 thin film acts as the "crystal seed", increasing the active sites and reducing the reduction barrier during cycling, similar to a prelithiated Li battery.[43]

4. CONCLUSIONS

In summary, we demonstrated that the EC performance and cyclic stability of Al^{3+}-based WO_3−NiO ECDs can be significantly improved by introducing an ALD−AZO interfacial layer. This leads to a shorter colored/bleached response time (5.8 s/4.2 s), along with exceptional cyclic stability (20,000 cycles) and capacitance retention (154.2%). The improved diffusion coefficient and reduced R_{ct} of the ALD−AZO/WO_3 thin film can be attributed to the effective regulation of the band gap of WO_3 and promotion of the electron transport process. Additionally, the introduction of ALD−AZO induces the formation of a robust SEI, protecting the electrode during cycling and enhancing the long-term cyclic stability of the ECDs. Therefore, the strategy of introducing an ALD−AZO interfacial layer holds great promise for enhancing the EC performance and cyclic stability of multivalent Al^{3+}-based ECDs.

■ ASSOCIATED CONTENT

Supporting Information

The Supporting Information is available free of charge at https://pubs.acs.org/doi/10.1021/acsami.4c00303.

UPS results of the AZO/WO_3 thin film, CV curves of the thin films, NiO thin film details, XRD results of the thin film, Raman results of thin films, C 1s XPS spectra, FFT results, EDX images, SEM images of the thin films, AFM images of the thin films, and comparison of stability between this work and other reported work (PDF)

■ AUTHOR INFORMATION

Corresponding Authors

Hongliang Zhang − *Laboratory of Advanced Nano Materials and Devices, Ningbo Institute of Materials Technology and Engineering, Chinese Academy of Sciences, Ningbo 315201, China;* orcid.org/0000-0002-9295-8683; Phone: +86 574 86688153; Email: zhanghl@nimte.ac.cn

https://doi.org/10.1021/acsami.4c00303
ACS Appl. Mater. Interfaces 2024, 16, 18164−18172

Jumei Zhou − *Faculty of Maritime and Transportation, Ningbo University, Ningbo 315211, China*; Email: zhoujumei@nbu.edu.cn

Authors

Shichen Weng − *Faculty of Maritime and Transportation, Ningbo University, Ningbo 315211, China; Laboratory of Advanced Nano Materials and Devices, Ningbo Institute of Materials Technology and Engineering, Chinese Academy of Sciences, Ningbo 315201, China*

Zhenhu Cao − *Ningbo Mi Ruo Electronic Technology Co. LTD, Ningbo 315203, China*

Kunrun Song − *Faculty of Maritime and Transportation, Ningbo University, Ningbo 315211, China; Laboratory of Advanced Nano Materials and Devices, Ningbo Institute of Materials Technology and Engineering, Chinese Academy of Sciences, Ningbo 315201, China*

Wentao Chen − *Ningbo Mi Ruo Electronic Technology Co. LTD, Ningbo 315203, China*

Ran Jiang − *Faculty of Maritime and Transportation, Ningbo University, Ningbo 315211, China*

Alexandr Alexandrovich Rogachev − *Optical Anisotropic Films Laboratory, Institute of Chemistry of New Materials of the National Academy of Sciences of Belarus, Minsk 220141, Belarus;* orcid.org/0000-0003-4993-0519

Maxim Anatolievich Yarmolenko − *Francisk Skorina Gomel State University, Gomel 246019, Belarus;* orcid.org/0000-0002-1283-8762

Complete contact information is available at: https://pubs.acs.org/10.1021/acsami.4c00303

Author Contributions

Shichen Weng: writing—original draft, validation, visualization, software, methodology, investigation, and data curation. Zhenhu Cao: project administration. Kunrun Song: data curation, visualization, and investigation. Wentao Chen: data curation, visualization, and investigation. Ran Jiang: methodology and investigation. A.A. Rogachev: validation. M.A. Yarmolenko: validation. Jumei Zhou: resources, supervision, and project administration. Hongliang Zhang: funding acquisition, methodology, project administration, resources, supervision, and writing—review and editing.

Notes

The authors declare no competing financial interest.

■ ACKNOWLEDGMENTS

This project is supported by the International Cooperation Project of Ningbo City, grant no. 2023H003.

■ REFERENCES

(1) Chen, M. J.; Zhang, X.; Yan, D. K.; Deng, J. B.; Sun, W. H.; Li, Z. T.; Xiao, Y. J.; Ding, Z. M.; Zhao, J. P.; Li, Y. Oxygen vacancy modulated amorphous tungsten oxide films for fast-switching and ultra-stable dual-band electrochromic energy storage smart windows. *Mater. Horiz.* **2023**, *10* (6), 2191−2203.

(2) Wang, S.; Xu, H. B.; Hao, T. T.; Wang, P. Y.; Zhang, X.; Zhang, H. M.; Xue, J. Y.; Zhao, J. P.; Li, Y. In situ XRD and operando spectra-electrochemical investigation of tetragonal WO_{3-x} nanowire networks for electrochromic supercapacitors. *NPG Asia Mater.* **2021**, *13* (1), 51.

(3) Zhang, H. L.; Zhang, X.; Sun, W. H.; Chen, M. J.; Xiao, Y. J.; Ding, Z. M.; Yan, D. K.; Deng, J. B.; Li, Z. T.; Zhao, J. P.; Li, Y. All-Solid-State Transparent Variable Infrared Emissivity Devices for Multi-Mode Smart Windows. *Adv. Funct. Mater.* **2023**, 2307356.

(4) Llordes, A.; Garcia, G.; Gazquez, J.; Milliron, D. J. Tunable near-infrared and visible-light transmittance in nanocrystal-in-glass composites. *Nature* **2013**, *500* (7462), 323−326.

(5) Pan, J. B.; Zheng, R. Z.; Wang, Y.; Ye, X. K.; Wan, Z. Q.; Jia, C. Y.; Weng, X. L.; Xie, J. L.; Deng, L. J. A high-performance electrochromic device assembled with hexagonal WO_3 and NiO/PB composite nanosheet electrodes towards energy storage smart window. *Sol. Energy Mater. Sol. Cells* **2020**, *207*, 110337.

(6) Zhang, H. L.; Liu, S.; Xu, T.; Xie, W. P.; Chen, G. X.; Liang, L. Y.; Gao, J. H.; Cao, H. T. Aluminum-ion-intercalation nickel oxide thin films for high-performance electrochromic energy storage devices. *J. Mater. Chem. C* **2021**, *9* (48), 17427−17436.

(7) Zhang, W.; Li, H. Z.; Al-Hussein, M.; Elezzabi, A. Y. Electrochromic Battery Displays with Energy Retrieval Functions Using Solution-Processable Colloidal Vanadium Oxide Nanoparticles. *Adv. Opt. Mater.* **2020**, *8* (2), 1901224.

(8) Cong, S.; Geng, F. X.; Zhao, Z. G. Tungsten Oxide Materials for Optoelectronic Applications. *Adv. Mater.* **2016**, *28* (47), 10518−10528.

(9) Wang, K.; Zhang, H. L.; Xie, W. P.; Chen, G. X.; Jiang, R.; Tao, K.; Liang, L. Y.; Gao, J. H.; Cao, H. T. Unraveling the Role of Water on the Electrochromic and Electrochemical Properties of Nickel Oxide Electrodes in Electrochromic Pseudocapacitors. *J. Electrochem. Soc.* **2021**, *168* (11), 113502.

(10) Wang, Z. H.; Zhang, X.; Zhang, H. L.; Ge, F. F.; Wang, Q.; Zhang, C. L.; Xu, G. L.; Gao, J. H.; Rogachev, A. A.; Cao, H. T. Real-Time Mass Change: An Intrinsic Indicator to Dynamically Probe the Electrochemical Degradation Evolution in WO_3. *Adv. Mater. Interfaces* **2022**, *9* (19), 2200340.

(11) Li, K. R.; Shao, Y. L.; Liu, S. Y.; Zhang, Q. H.; Wang, H. Z.; Li, Y. G.; Kaner, R. B. Aluminum-Ion-Intercalation Supercapacitors with Ultrahigh Areal Capacitance and Highly Enhanced Cycling Stability: Power Supply for Flexible Electrochromic Devices. *Small* **2017**, *13* (19), 1700380.

(12) Mak, A. K.; Tuna, O.⋯; Öztürk, O.; Karabulut, M. Comparison of Al^{3+} and Li^+ liquid electrolytes for as deposited and heat treated WO_3 thin films for electrochromic applications. *Solid State Ionics* **2022**, *386*, 116059.

(13) Zhang, S. L.; Cao, S.; Zhang, T. R.; Fisher, A.; Lee, J. Y. Al^{3+} intercalation/de-intercalation-enabled dual-band electrochromic smart windows with a high optical modulation, quick response and long cycle life. *Energy Environ. Sci.* **2018**, *11* (10), 2884−2892.

(14) Imanaka, N.; Kobayashi, Y.; Tamura, S.; Adachi, G. Trivalent Al^{3+} ion conduction in $Al_2(WO_4)_3$ solids. *Electrochem. Solid-State Lett.* **1999**, *1* (6), 271−273.

(15) Tamura, S.; Imanaka, N. Solid electrolyte-type gas sensors applied trivalent cation conducting solid electrolytes. *Sens. Actuators, B* **2022**, *368*, 132252.

(16) Li, H. Z.; McRae, L.; Firby, C. J.; Elezzabi, A. Y. Rechargeable Aqueous Electrochromic Batteries Utilizing Ti-Substituted Tungsten Molybdenum Oxide Based Zn^{2+} Ion Intercalation Cathodes. *Adv. Mater.* **2019**, *31* (15), 1807065.

(17) Hopmann, E.; Li, H. Z.; Elezzabi, A. Y. Rechargeable Zn^{2+}/Al^{3+} dual-ion electrochromic device with long life time utilizing dimethyl sulfoxide (DMSO)-nanocluster modified hydrogel electrolytes (vol 9, pg 32047, 2019). *RSC Adv.* **2019**, *9* (64), 37179.

(18) Wu, C.; Shi, H. S.; Zhao, L. Q.; Chen, X.; Zhang, X. S.; Zhang, C.; Yu, J. M.; Lv, Y. J.; Wei, R.; Gao, T. Y.; Xie, J.; Yu, Y.; Liu, W. High-Performance Aqueous Zn^{2+}/Al^{3+} Electrochromic Batteries based on Niobium Tungsten Oxides. *Adv. Funct. Mater.* **2023**, *33* (20), 2214886.

(19) Gao, Z. H.; Zhang, C. L.; Gao, J. H.; Wang, Q.; Xu, G. L.; Cao, H. T.; Zhang, H. L. Nucleation and growth of low resistivity copper thin films on polyimide substrates by low-temperature atomic layer deposition. *Appl. Surf. Sci.* **2023**, *638*, 158072.

(20) Zhao, F. L.; Dong, J. C.; Zhao, N. N.; Wu, J.; Han, D. D.; Kang, J. F.; Wang, Y. Characteristics of atomic layer deposited transparent aluminum-doped zinc oxide thin films at low temperature. *Rare Met.* **2016**, *35* (7), 509−512.

(21) Wang, K.; Zhang, H. L.; Chen, G. X.; Tian, T.; Tao, K.; Liang, L. Y.; Gao, J. H.; Cao, H. T. Long-term-stable WO_3-PB complementary electrochromic devices. *J. Alloys Compd.* **2021**, *861*, 158534.
(22) Song, K. R.; Weng, S. C.; Zhou, J. M.; Jiang, R.; Cao, H. T.; Zhang, H. L. Tunable Optical Constants of Aluminum Tungsten Bronzes in Electrochromic Tungsten Oxide Thin Films. *J. Phys. Chem. C* **2023**, *127* (36), 18036−18042.
(23) Wang, B. S.; Huang, Y.; Han, Y.; Zhao, S. M.; Ding, W. L.; Zhang, W. S.; Li, R.; Wu, X. K.; Jiang, Q. Y.; Li, Y. R.; Gao, D.; Zhao, Y. L.; Wang, F.; Jiang, H. R.; Zhang, R. F. Single tungsten atoms modified porous V_2O_5 nanoflowers with enhanced electrochromic performance. *Cell Rep. Phys. Sci.* **2023**, *4* (5), 101408.
(24) Wang, B. S.; Li, R. Y.; Zhang, Z. Y.; Zhang, W. W.; Yan, X. L.; Wu, X. L.; Cheng, G. A.; Zheng, R. T. Novel Au/Cu_2O multi-shelled porous heterostructures for enhanced efficiency of photoelectrochemical water splitting. *J. Mater. Chem. A* **2017**, *5* (27), 14415−14421.
(25) Wang, C. C.; Su, W. L. Ultrathin Artificial Solid Electrolyte Interface Layer-Coated Biomass-Derived Hard Carbon as an Anode for Sodium-Ion Batteries. *ACS Appl. Energy Mater.* **2022**, *5* (1), 1052−1064.
(26) Yan, C.; Xu, R.; Xiao, Y.; Ding, J. F.; Xu, L.; Li, B. Q.; Huang, J. Q. Toward Critical Electrode/Electrolyte Interfaces in Rechargeable Batteries. *Adv. Funct. Mater.* **2020**, *30* (23), 1909887.
(27) Lim, K.; Hagel, M.; Kuster, K.; Fenk, B.; Weis, J.; Starke, U.; Popovic, J.; Maier, J. Chemical stability and functionality of Al_2O_3 artificial solid electrolyte interphases on alkali metals under open circuit voltage conditions. *Appl. Phys. Lett.* **2023**, *122* (9), 093902.
(28) Wan, J.; Hao, Y.; Shi, Y.; Song, Y. X.; Yan, H. J.; Zheng, J.; Wen, R.; Wan, L. J. Ultra-thin solid electrolyte interphase evolution and wrinkling processes in molybdenum disulfide-based lithium-ion batteries. *Nat. Commun.* **2019**, *10*, 3265.
(29) Li, H. Z.; Firby, C. J.; Elezzabi, A. Y. Rechargeable Aqueous Hybrid Zn^{2+}/Al^{3+} Electrochromic Batteries. *Joule* **2019**, *3* (9), 2268−2278.
(30) Zhang, S.; Cao, S.; Zhang, T. R.; Lee, J. Y. Plasmonic Oxygen-Deficient $TiO_{(2-x)}$Nanocrystals for Dual-Band Electrochromic Smart Windows with Efficient Energy Recycling. *Adv. Mater.* **2020**, *32* (43), 2004686.
(31) Yu, X. Q.; Sun, J. P.; Tang, K.; Li, H.; Huang, X. J.; Dupont, L.; Maier, J. Reversible lithium storage in LiF/Ti nanocomposites. *Phys. Chem. Chem. Phys.* **2009**, *11* (41), 9497−9503.
(32) Wang, K.; Qiu, D.; Zhang, H. L.; Chen, G. X.; Xie, W. P.; Tao, K.; Bao, S. H.; Liang, L. Y.; Gao, J. H.; Cao, H. T. Boosting charge-transfer kinetics and cyclic stability of complementary WO_3-NiO electrochromic devices via SnO_x interfacial layer. *J. Sci.: Adv. Mater. Devices* **2021**, *6* (3), 494−500.
(33) Wen, R. T.; Niklasson, G. A.; Granqvist, C. G. Strongly Improved Electrochemical Cycling Durability by Adding Iridium to Electrochromic Nickel Oxide Films. *ACS Appl. Mater. Interfaces* **2015**, *7* (18), 9319−9322.
(34) Fleisch, T. H.; Mains, G. J. AN XPS STUDY OF THE UV REDUCTION AND PHOTOCHROMISM OF MoO_3 AND WO_3. *J. Chem. Phys.* **1982**, *76* (2), 780−786.
(35) Jung, S. C.; Han, Y. K. How Do Li Atoms Pass through the Al_2O_3 Coating Layer during Lithiation in Li-ion Batteries? *J. Phys. Chem. Lett.* **2013**, *4* (16), 2681−2685.
(36) Xing, L. D.; Zheng, X. W.; Schroeder, M.; Alvarado, J.; von Wald Cresce, A.; Xu, K.; Li, Q. S.; Li, W. S. Deciphering the Ethylene Carbonate-Propylene Carbonate Mystery in Li-Ion Batteries. *Acc. Chem. Res.* **2018**, *51* (2), 282−289.
(37) Dai, X. Y.; Zhou, A. J.; Xu, J.; Yang, B.; Wang, L. P.; Li, J. Z. Superior electrochemical performance of $LiCoO_2$ electrodes enabled by conductive Al_2O_3-doped ZnO coating via magnetron sputtering. *J. Power Sources* **2015**, *298*, 114−122.
(38) Lee, G. B.; Song, S. H.; Lee, M. W.; Kim, Y. J.; Choi, B. H. Characterization of physical and mechanical properties of Al_2O_3-doped ZnO (AZO) thin films deposited on transparent polyimide supports with various ALD process parameters. *Appl. Surf. Sci.* **2021**, *535*, 147731.
(39) Chen, Y.; Pan, H. D. A.; Lin, C.; Li, J. X.; Cai, R. S.; Haigh, S. J.; Zhao, G. Y.; Zhang, J. M.; Lin, Y. B.; Kolosov, O. V.; Huang, Z. G. Controlling Interfacial Reduction Kinetics and Suppressing Electrochemical Oscillations in $Li_4Ti_5O_{12}$ Thin-Film Anodes. *Adv. Funct. Mater.* **2021**, *31* (43), 2105354.
(40) Duffy, J. A.; Ingram, M. D.; Monk, P. M. S. THE EFFECT OF MOISTURE ON TUNGSTEN-OXIDE ELECTROCHROMISM IN POLYMER ELECTROLYTE DEVICES. *Solid State Ionics* **1992**, *58* (1−2), 109−114.
(41) Lipson, A. L.; Puntambekar, K.; Comstock, D. J.; Meng, X. B.; Geier, M. L.; Elam, J. W.; Hersam, M. C. Nanoscale Investigation of Solid Electrolyte Interphase Inhibition on Li-Ion Battery MnO Electrodes via Atomic Layer Deposition of Al_2O_3. *Chem. Mater.* **2014**, *26* (2), 935−940.
(42) Liu, J.; Sun, X. L. Elegant design of electrode and electrode/electrolyte interface in lithium-ion batteries by atomic layer deposition. *Nanotechnology* **2015**, *26* (2), 024001.
(43) Wang, Z. H.; Zhang, L. L.; Zhang, H. L.; Jiang, R.; Liang, L. Y.; Gao, J. H.; Cao, H. T. Mechanistic insights into the dry prelithiated WO_3 thin films in electrochromic devices. *Solid State Ionics* **2021**, *373*, 115814.

https://doi.org/10.1021/acsami.4c00303
ACS Appl. Mater. Interfaces 2024, 16, 18164−18172